

Communication

## Allosteric Inhibitors, Crystallography and Comparative Analysis Reveal Network of Coordinated Movement Across Human Herpesvirus Proteases

Timothy M Acker, Jonathan E. Gable, Markus-Frederik Bohn, Priyadarshini Jaishankar, Michael C. Thompson, James S. Fraser, Adam R. Renslo, and Charles S. Craik

*J. Am. Chem. Soc.*, **Just Accepted Manuscript** • DOI: 10.1021/jacs.7b04030 • Publication Date (Web): 31 Jul 2017

Downloaded from <http://pubs.acs.org> on August 7, 2017

### Just Accepted

“Just Accepted” manuscripts have been peer-reviewed and accepted for publication. They are posted online prior to technical editing, formatting for publication and author proofing. The American Chemical Society provides “Just Accepted” as a free service to the research community to expedite the dissemination of scientific material as soon as possible after acceptance. “Just Accepted” manuscripts appear in full in PDF format accompanied by an HTML abstract. “Just Accepted” manuscripts have been fully peer reviewed, but should not be considered the official version of record. They are accessible to all readers and citable by the Digital Object Identifier (DOI®). “Just Accepted” is an optional service offered to authors. Therefore, the “Just Accepted” Web site may not include all articles that will be published in the journal. After a manuscript is technically edited and formatted, it will be removed from the “Just Accepted” Web site and published as an ASAP article. Note that technical editing may introduce minor changes to the manuscript text and/or graphics which could affect content, and all legal disclaimers and ethical guidelines that apply to the journal pertain. ACS cannot be held responsible for errors or consequences arising from the use of information contained in these “Just Accepted” manuscripts.

1

# Allosteric Inhibitors, Crystallography and Comparative Analysis Reveal Network of Coordinated Movement Across Human Herpesvirus Proteases

Timothy M. Acker<sup>1</sup>, Jonathan E. Gable<sup>1</sup>, Markus-Frederik Bohn<sup>1</sup>, Priyadarshini Jaishankar<sup>1</sup>, Michael C. Thompson<sup>2</sup>, James S. Fraser<sup>2</sup>, Adam R. Renslo<sup>1</sup>, Charles S. Craik<sup>1</sup>

<sup>1</sup>Department of Pharmaceutical Chemistry, University of California, San Francisco, California 94158, United States  
University of California San Francisco

<sup>2</sup>Department of Bioengineering and Therapeutic Sciences, University of California, San Francisco, California 94158, United States

*Supporting Information Placeholder*

**ABSTRACT:** Targeting of cryptic binding sites represents an attractive but underexplored approach to modulating protein function with small molecules. Using the dimeric protease (Pr) from Kaposi's sarcoma-associated herpesvirus (KSHV) as a model system, we sought to dissect a putative allosteric network linking a cryptic site at the dimerization interface to enzyme function. Five cryogenic x-ray structures were solved of the monomeric protease with allosteric inhibitors bound to the dimer interface site. Distinct coordinated movements captured by the allosteric inhibitors were also revealed as alternative states in room temperature X-ray data and comparative analyses of other dimeric herpesvirus proteases. A two-step mechanism was elucidated through detailed kinetic analyses and suggests an enzyme isomerization model of inhibition. Finally, a representative allosteric inhibitor from this class was shown to be efficacious in a cellular model of viral infectivity. These studies reveal a coordinated dynamic network of atomic communication linking cryptic binding site occupancy and allosteric inactivation of KSHV Pr that can be exploited to target other members of this clinically relevant family of enzymes.

Infection by one or more of the nine herpesvirus family members is prevalent in the global population.<sup>1</sup> While severity of infection varies by herpesvirus subtype, these infections contribute significantly to morbidity and their effective treatment remains an important unmet clinical need. There are numerous programs aimed at developing therapeutics and elucidating new drug targets for Human herpesviridae (HHV).<sup>2</sup> One potential therapeutic strategy, of blocking the herpesvirus protease, has been validated through genetic knock-out and knock-down.<sup>3</sup> There have been previous efforts aimed at targeting the non-canonical His-His-Ser catalytic triad that is conserved across the HHV proteases.<sup>2</sup>

We aimed to target a cryptic binding site that is accessed after rotameric state changes in Trp109 of KSHV protease (KSHV Pr).<sup>4</sup> Targeting cryptic binding sites can be challenging, since endogenous ligands for these sites are not typically available, nor

is the functional effect of engaging such sites known *a priori*. Therefore, understanding how cryptic sites form, bind non-native small molecule ligands, and communicate with the rest of the protein is an active area of research, both computationally and experimentally.<sup>5</sup> However, there are few experimentally validated systems where cryptic pockets have been exploited for drug design.

In this study, small molecules, kinetics, and cryogenic and room temperature x-ray crystallography were used to understand novel inhibitors that trap an inactive conformational state. Comparative analysis across the herpesvirus family identified an allosteric circuit linking distal loop regions, helix five, the cryptic binding site and the active site. We further describe the kinetic mechanism of inhibition by these compounds, elucidating a slow, two-step mechanism of inhibition. Finally, for the first time, we demonstrate cellular efficacy with an allosteric inhibitor, suggesting that engaging this cryptic binding site is a viable strategy for inhibiting herpesvirus infectivity.

The KSHV Pr dimer (Figure 1A) is known to form via a concentration dependent disorder to order transition of helix five and six that drive dimerization and catalytic competency. We previously described first-in-class allosteric inhibitors of KSHV that engage this dimerization interface by projecting two hydrophobic side chains from a rigid picolinamide scaffold (Figure 1A).<sup>4</sup> This scaffold has been shown to exhibit mixed inhibition and similar results were obtained with compounds in this study (Supplemental Table 3).<sup>4</sup> To more fully understand the nature of the transient, cryptic binding pocket engaged by this class of compounds, we varied the nature and connectivity of the hydrophobic side chains R<sup>1</sup> and R<sup>2</sup> that project into the cryptic binding site within KSHV Pr (Figure 1B, Supplemental Tables 1 and 2).

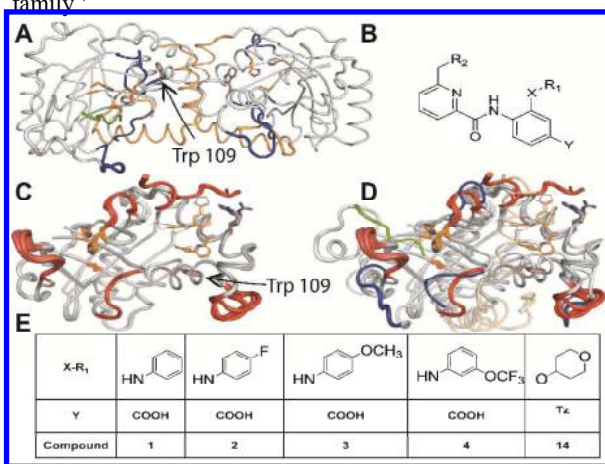
Changing the benzylic R1 side chain to aniline (X: CH<sub>2</sub> → NH) was well tolerated and enabled ready access to analogs with differentially substituted R1 moieties. The introduction of small substituents on the aniline ring afforded analogs with IC<sub>50</sub> values between 2.5 and 5.4 μM (Supplemental Table 1) in a biochemical

2

1 assay of KSHV Pr enzymatic activity, and were similar in potency  
 2 to the original inhibitors. Somewhat improved potencies, in the  
 3 sub-micromolar regime, were achieved by replacing the aniline  
 4 side chain with ether or thio-ether linked aliphatic or  
 5 heteroaliphatic rings at R1.

6 We next explored modification of the R2 side chain in the  
 7 background of preferred alicyclic R1 groups like cyclohexyl,  
 8 pyran, and thiopyran, and with further replacement of the  
 9 carboxylate by the common acid bioisostere tetrazole. At R2 we  
 10 prepared analogs with the original cyclohexylmethyl side chain,  
 11 as well as several analogs with mono- or di-substituted benzylic  
 12 side chains (Supplemental Table 2). These analogs exhibited a  
 13 broader range of IC<sub>50</sub> values ranging from 0.7–13.1 μM. We  
 14 found that increasing hydrophobicity of the R1 side chain  
 15 improved potencies in the order pyran < thiopyran < cyclohexyl  
 16 (most potent, Figure S1). By contrast, changes made to the R2  
 17 side chain did not impact potency significantly (Supplemental  
 18 Table 2).

19 We successfully co-crystallized five new compounds (Figure 1B,  
 20 C and D) in complex with a C-terminal Δ196 construct of the  
 21 protease.<sup>4b, 6</sup> These X-ray crystal structures have resolution  
 22 ranging between 1.8 and 2.1 Å (See Supplemental). Importantly,  
 23 these structures revealed conformations of the C-terminal region  
 24 and two distal loop regions, that are distinct as compared to the  
 25 previously reported dimeric structure 2PBK (Figure 1B). The  
 26 conformation of the oxyanion hole is rendered the active site  
 27 incompetent for catalysis (Figure 1C).<sup>4b</sup> It is notable that the  
 28 conformation of the oxyanion hole in these experiments differs  
 29 from that of an apo-monomeric protease from the alpha-  
 30 herpesvirus family.<sup>7</sup>



31 **Figure 1.** Binding of small molecules to the cryptic binding  
 32 pocket leads to coordinated rearrangements of distal sites at  
 33 the protein. **A.** The KSHV protease dimer (PDB: 2PBK) is shown  
 34 with the dimer interface helices in orange. Trp109 is shown  
 35 in brown and blue and is located behind helix 5. The active site  
 36 residues are shown in orange and the loop regions that adopt  
 37 distinct conformations in the compound bound monomers are  
 38 shown in blue. **B.** The small-molecule scaffold with variable R-  
 39 group regions is shown, where Y is either COOH or a tetrazole  
 40 (Tz). **C.** The cryogenic co-crystal structures solved (PDB codes:  
 41 SUR3, 5UVP, 5UV3, 5UTE, 5UTN) in this study are overlaid.  
 42 The dynamic loop regions are shown in red, scaled to their B-  
 43 factors and the compounds are shown in orange. **D.** One monomer  
 44 from the dimer structure (2PBK) is overlaid with a monomer from  
 45 this study. Several loops from the monomeric structures, shown in  
 46 red, are in distinct conformations from those of the dimeric  
 47 structure shown in blue. **E.** The R1 groups from compounds that

are co-crystallized in this study are shown (benzyl (1), 4-F-Benzyl  
 (2), 4-OCH<sub>3</sub>-Benzyl (3), 3-OCF<sub>3</sub>-Benzyl (4), tetrahydropyran  
 (14), **Note:** R2 is cyclohexyl for each of the co-crystallized  
 compounds. (This figure is enlarged in the Supplemental  
 Material)

Across all molecules, the C-terminus adopts one of two  
 conformations, both of which make critical but distinct H-bonds  
 with the ligand. The co-crystal structure of **1** is representative of  
 the first conformation (Figure S2A), which has two hydrogen  
 bonding networks, one between the backbone residues (193 thru  
 195) and the carboxylic acid of the molecules, and one through  
 the carboxylic acid of the small molecules and the side chain  
 residues of T195 and R82 (Figure S2). This conformation  
 represents a significant rearrangement of the residues as compared  
 to the orientation in previously reported structures. In contrast, **14**  
 adopts a distinct pattern where the C-terminal residues are  
 directed away from the small molecule, in a similar trajectory to  
 that of the dimeric structures (Figure S2B). These two  
 conformations change the overall shape of the cryptic allosteric  
 pocket and the solvent accessible surface area is decreased in the  
 extended conformation exemplified by **1** (Figure 2A, B).

To test the idea that these two conformations of the C-terminus  
 were nearly iso-energetic, we used room temperature data

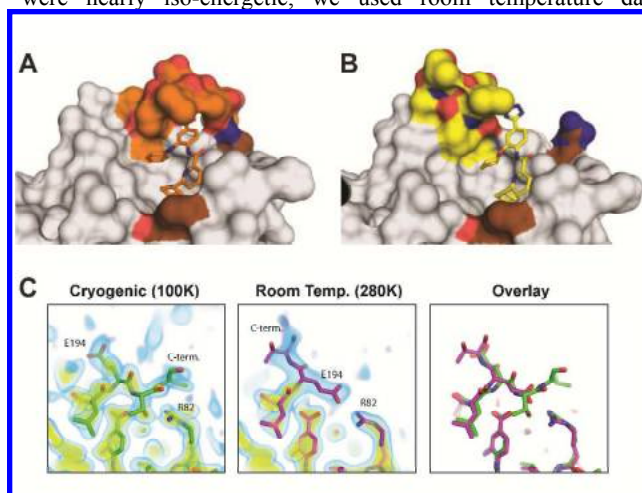


**Figure 2.** Distinct C-terminal conformations are identified in this  
 study. **A.** Compound **1** cryogenic co-crystal structure with the  
 surface representation shown. The orientation of the C-terminal  
 residues forms a well-defined pocket that encapsulates the  
 compound. **B.** Compound **14** cryogenic co-crystal structure with  
 the surface representation shown. The orientation of the C-  
 terminal residues leaves the anion exposed to solvent and is in a  
 similar trajectory to that of the dimeric helices. **C.** Electron  
 density supporting temperature-dependent conformational  
 differences between structures determined at 100K and 280K  
 (280K PDB codes: 5V5D, 5V5E). The leftmost column of panel  
 shows an electron density map and model derived from cryogenic  
 (100K, Compound 4) data, the middle panel shows maps and  
 models derived from room temperature (280K, Compound 4)  
 data, and the rightmost panel shows overlays of the 100K and  
 280K models. The electron density maps are calculated using  
 2Fo-Fc amplitudes with model phases and are contoured at 2.5σ  
 (yellow) or 1.0σ (blue). A nearly 180° rotation of the φ-angle of  
 Glu194 positions the C-terminus in opposite directions in each of  
 the two structures, leading to a slightly different set of  
 interactions stabilizing the cryptic binding site.

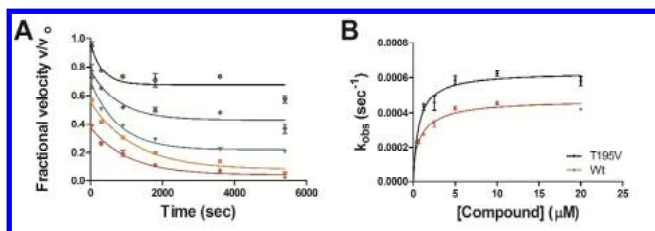
collection to avoid artifacts associated with cryo-cooling.<sup>8</sup> The

3

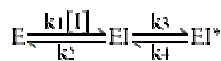
1 cryogenic and 280K structures of the protease bound to compound  
 2 **4** show substantial differences where the C-terminus of the  
 3 protease adopts a conformation that differs from the cryogenic  
 4 structure by a 180° rotation of the  $\phi$ -angle of Glu194 (Figure 2C).  
 5 This structural rearrangement orients the C-terminus differently  
 6 and alters polar interactions that form the cryptic binding site and  
 7 places the carboxylate of E194 in close proximity to the  
 8 guanidinium group of R82. The observation of these temperature-  
 9 dependent conformational differences suggests that the protease  
 10 retains considerable flexibility when bound to compound **4**. This  
 11 additional conformation is similar to the conformation observed  
 12 when bound to molecules such as **14**.

13 These structural observations led us to further explore the  
 14 relationship between the dynamic regions within the co-crystal  
 15 series developed here and across the ensemble of 24 published  
 16 herpesvirus protease crystal structures. We calculated the RMSD  
 17 and RMSF between the structures (Figure S3A, B). Notably, the  
 18 loop regions identified above (residues 15-23, 80-100 and the  
 19 oxyanion hole loop) show the largest root mean square  
 20 fluctuations (RMSF) across the analysis. One way to identify  
 21 whether these regions exhibiting conformational variability are  
 22 coordinated is with principal component analysis (PCA) of  $C\alpha$   
 23 distances among these similar structures (Figure S2C). The  
 24 regions showing the largest RMSF are captured by principal  
 25 component one, suggesting these motions are coordinated across  
 26 the structures evaluated here. The combination of allosteric acting  
 27 small molecules and their co-crystal structures therefore  
 28 potentially inform the identification of the link between allosteric  
 29 regulation of catalysis and the overall network of atomic  
 30 communication across distal regions of the protein throughout the  
 31 herpesvirus family.

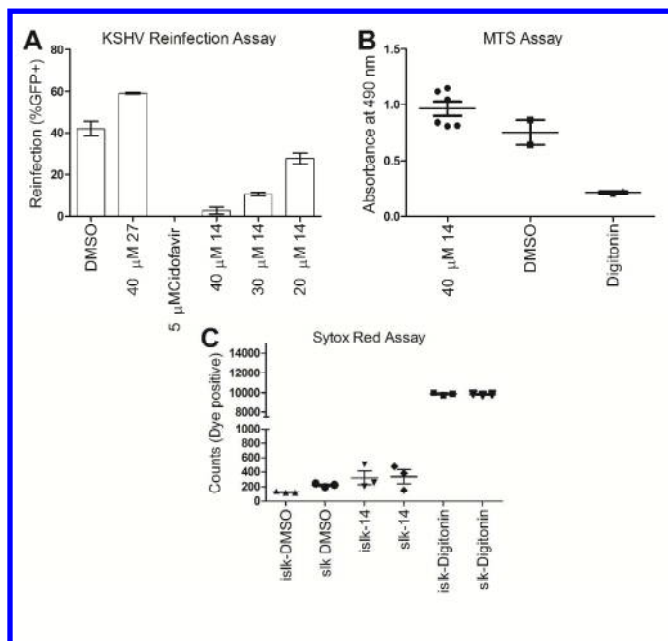
32 During our elaboration of the structure activity relationships  
 33 (SAR) of compound congeners, we observed a time-dependence  
 34 of inhibition with the compounds. We therefore evaluated the  
 35 progress curves of the full reactions, beginning with the fractional  
 36 velocity (Figure 3A). It is apparent that there is a rapid,  
 37 concentration-dependent inhibition during this analysis, followed  
 38 by a slow increase in inhibition over time. These observations  
 39 suggest a possible two-step model of enzyme isomerization as a  
 40 mechanism of inhibition. Fitting the full progress curves of the  
 41 reaction for  $k_{obs}$  as a function of inhibitor concentration using the  
 42 equation  $[P] = v_s * t + ((v_i - v_s) / k_{obs}) (1 - \exp(-k_{obs} * t))$ , where  $P$   
 43 is derived from the increase in fluorescence and  $t$  is time, reveals a  
 44 hyperbolic increase in  $k_{obs}$  (Figure 4B). This observation supports



45 **Figure 3.** Compounds display slow time-dependent inhibition and  
 46 two-step inhibition. **A.** The fractional velocity of the reactions  
 47 shows that there is a rapid, concentration dependent inhibition  
 48 followed by a slow onset to the steady-state. The curves are from  
 49 a two-fold dilution scheme beginning at 25  $\mu$ M (red) and ending  
 50 at 1.6  $\mu$ M (black) of compound **14**. **B.** Fitting the progress curves  
 51 for  $k_{obs}$  shows a hyperbolic fit for the compounds, supporting a  
 52 two-step enzyme isomerization mechanism of inhibition. The data  
 53 shown are for compound **1**.



an enzyme isomerization model, e.g.  
 where  $E$  is the protease monomer,  $EI$  is the initial encounter  
 complex and  $EI^*$  represents an enzyme isomerization event, with  
 the  $k_{obs}$  values from each concentration fitting the equation  
 $k_{obs} = k_3 + ((k_4 [X]) / (K_i + [X]))$ , where  $[X]$  is the inhibitor  
 concentration.<sup>9</sup> The fitted  $K_i$  (note that  $K_i$  here is for the initial  
 encounter complex) values are in good agreement with the fitted  
 $IC_{50}$  values (Compound **1**:  $IC_{50}$  5.4  $\mu$ M,  $K_i = 1.2 \pm 0.7$   $\mu$ M,  $k_3 =$   
 $0.0003 \pm 0.00008$   $sec^{-1}$ ,  $k_4 = 0.0001 \pm 0.00007$   $sec^{-1}$ , Compound  
**14**:  $IC_{50}$  3.6  $\mu$ M,  $K_i = 0.4 \pm 3$   $\mu$ M,  $k_3 = 0.0003 \pm 0.001$   $sec^{-1}$ ,  $k_4 =$   
 $0.0002 \pm 0.001$   $sec^{-1}$ , Figure 5B). We note that the error associated  
 with these fits is relatively large due to the very slow nature of the  
 observed kinetics and the intrinsic variability in the assay system.  
 We therefore chose to use pre-incubation and  $IC_{50}$  as the readout  
 in our SAR campaigns, as the modest tight-binding inhibition was  
 challenging to fit (See Supplemental Methods). We also verified  
 the reversible nature of inhibition with rapid dilution and dialysis  
 experiments (Data not shown). However, the enzyme  
 isomerization model of inhibition fits with the observed structural  
 rearrangements of the enzyme and the dynamic long range  
 coordinated networks observed in this study. When we mutated  
 T195 to V195 (Figure 3B) in order to disrupt the hydrogen  
 bonding network between the side chain residue and the  
 carboxylic acid of the small molecules, we observe an increase in  
 the rate for  $k_{obs}$ . This observation suggests that the isomerization  
 can happen faster, due to less ordering of the disordered residues,  
 a phenomenon which is known to occur when shifting equilibrium  
 toward the monomer.



54 **Figure 4.** Cellular evaluation of a tetrazole compound **14**. **A.**  
 55 Compound **14** displays concentration dependent inhibition in  
 56 re-infectivity as compared to DMSO. An inactive congener  
 57 shows no inhibition of re-infectivity. Cidofavir is included as a  
 58 positive control. **B.** Cell viability, as measured by MTS assay  
 59 shows no significant differences between compound treated  
 60 and DMSO control. Digitonin served as a positive control. **C.**  
 The Sytox red assay for membrane permeability shows no  
 significant differences between compound-treated and DMSO-  
 treated cells for the iSLK and SLK cells.

4

1 Finally, the tetrazole isostere was envisioned as a candidate for  
2 cellular studies due to the distribution of the negative charge  
3 through the nitrogenous ring and a favorable cLogD (pH8.0) of  
4 2.14. This compound was evaluated for efficacy in an established  
5 model of cellular re-infectivity using the iSLK.219 and SLK cells  
6 (Figure 4). The iSLK.219 cells are stably infected doxycycline  
7 (DOX) inducible KSHV+ cells (See Supplemental Methods).  
8 Treatment with compound **14** resulted in a dose dependent  
9 decrease in re-infectivity as measured by flow cytometry (Figure  
10 4A, cellular EC<sub>50</sub> 23.6 μM, 95% confidence interval 22.6 to 24.6  
11 μM). The inhibition was compound specific, with a related,  
12 biochemically inactive analog (**27**, See Supplemental) eliciting no  
13 decrease in the re-infection readout. The potential off-target  
14 cellular effects of compound **14** were evaluated using two  
15 methods. First, cell viability was assessed using a MTS assay  
16 (Figure 4B). There were no significant changes in metabolism or  
17 proliferation due to the presence of the analog as compared to the  
18 DMSO controls (p > 0.05, one-way ANOVA, Bonferroni post-  
19 hoc analysis). Finally, the membrane permeability of the cells was  
20 assessed using the SYTOX red assay. There was no significant  
21 increase in permeability over the DMSO controls (Figure 4C, p >  
22 0.05 one-way ANOVA, Bonferroni post-hoc analysis).

23 Exploiting cryptic binding pockets in proteins that form protein-  
24 protein interactions presents an attractive therapeutic strategy for  
25 these challenging targets. This work advances our understanding  
26 of one such example and clearly establishes a link between cryptic  
27 pocket binding and long-range atomic communication. The  
28 opportunity to maintain the bound state via slow off rates at  
29 cryptic sites near protein interfaces otherwise requiring high  
30 surface area of binding holds the potential to allow small-  
31 molecule drug-like compounds to make further progress in  
32 modulating these challenging targets.

33 This study describes various cryogenic and room temperature co-  
34 crystal structures that, through comparative analysis, identify the  
35 distal regions most likely associated with the allosteric pathway of  
36 atomic communication across the herpesvirus family of proteases.  
37 Our analysis further suggests that the cryptic binding pocket shape  
38 is not rigid across the compound series assessed here, indeed  
39 temperature dependence suggests residual plasticity of distinct H-  
40 bonding patterns between the C-terminus and ligand can be  
41 further optimized to create more potent molecules. Both this  
42 plasticity and the analysis of the ensemble of all related proteases  
43 are consistent with the two-step mechanism of inhibition and  
44 induced fit type kinetics that we observe.

45 Finally, we establish cellular efficacy with this class of small  
46 molecules, which supports the idea that allosteric targeting of the  
47 herpesvirus proteases could be a tractable therapeutic strategy.  
48 The observed efficacy with the compounds represents a  
49 significant step forward in the pursuit of novel therapeutic  
50 strategies against human herpesviruses. We believe that the link  
51 between protein-protein interaction and the resulting allosteric  
52 networks that the herpesvirus family of proteases relies on  
53 presents an opportunity to target other viruses in a similar manner.

## 54 ASSOCIATED CONTENT

### 55 Supporting Information

56 The supporting information file (PDF) contains materials  
57 referenced in the above text and materials and methods for each of  
58 the experiments described above.

59 The Supporting Information is available free of charge on the  
60

ACS Publications website.

## AUTHOR INFORMATION

### Corresponding Author

Charles S. Craik, Department of Pharmaceutical Chemistry,  
University of California, San Francisco, California 94158, United  
States University of California San Francisco. Email:  
Charles.Craik@ucsf.edu, Phone: 415-476-8146

### Author Contributions

All authors contributed to the writing and editing of the  
manuscript and presentation of results.

### Notes

The authors declare no competing financial interests.

## ACKNOWLEDGMENT

We would like to acknowledge Christopher A. Waddling for  
helpful discussions, as well as Andrew Van Benschoten for  
assistance with room temperature data collection. We would also  
like to acknowledge the National Institutes of Health for funding:  
(R01-AI090592 to CSC, 1F32GM111012 to TMA). JEG was  
supported by NIH Structural Biology Training Grant GM008284  
and the National Science Foundation Graduate Research  
Fellowship Program (1144247).

## REFERENCES

1. Human Herpesviruses: Biology, Therapy, and Immunoprophylaxis. Arvin A, Gabriella, C.-F., Mocarski E, Moore, P.S., Roizman, B., Whitely, R., Yamanishi, K. editors., Ed. Cambridge University Press: Cambridge, 2007. <https://www.ncbi.nlm.nih.gov/books/NBK47376/>.
2. Gable, J. E.; Acker, T. M.; Craik, C. S. *Chem. Rev.* **2014**, 114 (22), 11382-11412.
3. Preston, V. G.; Coates, J. A. V.; Rixon, F. J. *J Virol* **1983**, 45 (3), 1056-1064.
4. (a) Shahian, T.; Lee, G. M.; Lazic, A.; Arnold, L. A.; Velusamy, P.; Roels, C. M.; Guy, R. K.; Craik, C. S. *Nat Chem. Biol.* **2009**, 5 (9), 640-646; (b) Lee, G. M.; Shahian, T.; Baharuddin, A.; Gable, J. E.; Craik, C. S. *J. Mol. Biol.* **2011**, 411 (5), 999-1016.
5. Cimermancic, P.; Weinkam, P.; Rettenmaier, T. J.; Bichmann, L.; Keedy, D. A.; Woldeyes, R. A.; Schneidman-Duhovny, D.; Demerdash, O. N.; Mitchell, J. C.; Wells, J. A.; Fraser, J. S.; Sali, A. *J. Mol. Biol.* **2016**, 428 (4), 709-719.
6. Gable, J. E.; Lee, G. M.; Jaishankar, P.; Hearn, B. R.; Waddling, C. A.; Renslo, A. R.; Craik, C. S. *Biochem* **2014**, 53 (28), 4648-4660.
7. Zuehlsdorf, M.; Werten, S.; Klupp, B.G.; Palm, G. J.; Mettenleiter, T. C.; Hinrichs, W. *PLoS Pathog.* **2015**, 11, 1-23.
8. Fraser, J. S.; van den Bedem, H.; Samelson, A. J.; Lang, P. T.; Holton, J. M.; Echols, N.; Alber, T. *Proc. Natl. Acad. Sci.* **2011**, 108 (39), 16247-16252.
9. Morrison, J. F.; Walsh, C. T. *Advances in Enzymology and Related Areas of Molecular Biology* **1988**, 61, 201-301.



5

